Simulations of Radiative Transfer in Combustion Systems and Further Developments of High-Order Spherical Harmonics Methods

Wenjun Ge

Department of Mechanical Engineering
School of Engineering
University of California, Merced
Merced, CA 95343, USA

wge@ucmerced.edu

Advanced Modeling & Simulation Seminar Series
NASA Ames Research Center
May 2, 2017

Outline

Outline

Combustion and combustion simulations

- Combustion is a chemical process in which a fuel reacts rapidly with oxygen and gives off heat.

- High-fidelity simulations: chemistry, turbulence, radiation and their interactions.

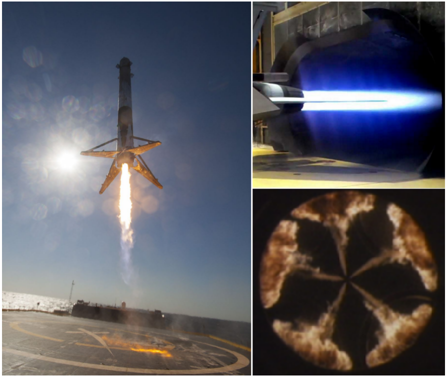

Source: left from SpaceX, top-right from internet
bottom-right from Imamori, Y. et al., 2011

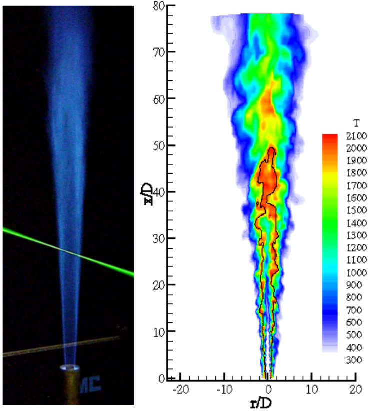

Source: left from Sandia NL, right from Pitsch, H., 2006

Radiative transfer

- Radiative transfer → electromagnetic waves → spectral dependence and travelling at 3×10^8 m/s in vacuum
- The radiative energy emitted by a blackbody is proportional to the fourth power of temperature → importance in high-temperature applications, nonlinearity
- Radiative transfer in participating/particulate media → emission, absorption and scattering → directional dependence

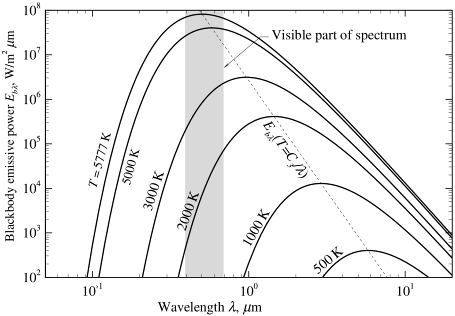

Figure : Blackbody emissive power spectrum.

- $E_b(T) = \int E_{b\lambda} d\lambda = n^2 \sigma_{SB} T^4$.
- Combustion problems generally involve temperature levels between 500 K and 2800 K so that the spectral ranges of interest in combustion applications are from 0.7μm to 30μ m (or 300∼14000 cm^{-1} in wavenumber).

- Vibration-rotation bands from bound-bound transitions
- The broadening of the spectral lines due to collisions and Doppler effect
- Modern databases: HITEMP, HITRAN, CDSD.
- $\kappa_\eta(\mathbf{Y}, T, p)$

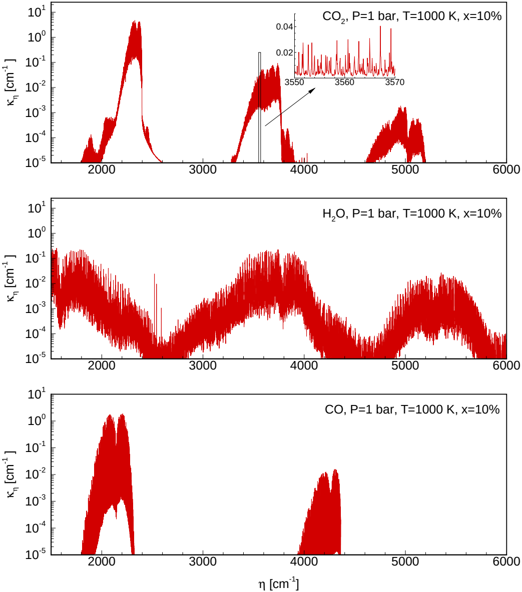

Radiative transfer equation (RTE) and radiative heat source

Radiative transfer in an absorbing, emitting and scattering medium is formulated by considering conservation of radiative energy, known as the radiative transfer equation (RTE).

RTE:

$$\hat{\mathbf{s}} \cdot \nabla_\tau I_\eta + I_\eta = (1 - \omega_\eta) I_{b\eta} + \frac{\omega}{4\pi} \int_{4\pi} I_\eta(\hat{\mathbf{s}}') \Phi_\eta(\hat{\mathbf{s}} \cdot \hat{\mathbf{s}}') d\Omega'$$

The net energy balance at any location in the medium is obtained by integrating the spectral intensity over all directions and all wavenumbers. The radiative heat source S_{rad}, is the difference between local absorption and emission:

Radiative heat source:

$$S_{rad} = -\nabla \cdot \mathbf{q}_{rad} = -S_{emi} + S_{abs} = -4\kappa_P \sigma_{SB} T^4 + \int_0^\infty \kappa_\eta \int_{4\pi} I_\eta(\boldsymbol{\tau}, \hat{\mathbf{s}}) \mathrm{d}\Omega \mathrm{d}\eta$$

Coupling to the energy equation for turbulent reacting flows

DNS (direct numerical simulation):

$$\frac{\partial \rho h}{\partial t} + \frac{\partial \rho h u_i}{\partial x_i} = -\frac{\partial J_i^h}{\partial x_i} + \frac{Dp}{Dt} + \tau_{ij}\frac{\partial u_j}{\partial x_i} + S_{rad}$$

LES (large eddy simulation):

$$\frac{\partial \bar{\rho}\tilde{h}}{\partial t} + \frac{\partial \bar{\rho}\tilde{h}\tilde{u}_i}{\partial x_i} = \frac{\partial(\bar{\rho}\tilde{h}\tilde{u}_i - \bar{\rho}\widetilde{hu_i})}{\partial x_i} - \frac{\partial \overline{J_i^h}}{\partial x_i} + \frac{D\bar{p}}{Dt} + \overline{\tau_{ij}\frac{u_j}{x_i}} + \overline{S_{rad}}$$

RANS (Raynolds-Averaged Navier-Stokes):

$$\frac{\partial \langle\rho\rangle\tilde{h}}{\partial t} + \frac{\partial \langle\rho\rangle\tilde{h}\tilde{u}_i}{\partial x_i} = \frac{\partial(\langle\rho\rangle\tilde{h}\tilde{u}_i - \langle\rho\rangle\widetilde{hu_i})}{\partial x_i} - \frac{\partial \langle J_i^h\rangle}{\partial x_i} + \frac{D\langle p\rangle}{Dt} + \langle\tau_{ij}\frac{u_j}{x_i}\rangle + \langle S_{rad}\rangle$$

Turbulence-radiation interaction (TRI)

Time-averaged radiative source $\langle S_{rad}\rangle$ accounting for turbulence effects:

$$\langle S_{rad}\rangle = -\langle S_{emi}\rangle + \langle S_{abs}\rangle = -4\pi\sigma_{SB}\langle \kappa_P I_b\rangle + \int_0^\infty \int_{4\pi} \langle \kappa_\eta I_\eta\rangle d\Omega d\eta$$

Emission TRI and absorption TRI:

Emission TRI: $\langle \kappa_P I_b\rangle \neq \kappa_P(\langle\phi\rangle) I_b(\langle T\rangle)$

Absorption TRI: $\langle \kappa_\eta I_\eta\rangle \neq \kappa_\eta(\langle\phi\rangle) I_\eta(\langle\phi\rangle)$

e.g. autocorrelation of I_b:

$$\mathcal{R}_{I_b} = \frac{I_b(\langle T\rangle)}{\langle I_b(T)\rangle} = \frac{(\langle T\rangle)^4}{\langle T^4\rangle} \neq 1$$

Interactions between radiation and reacting flow

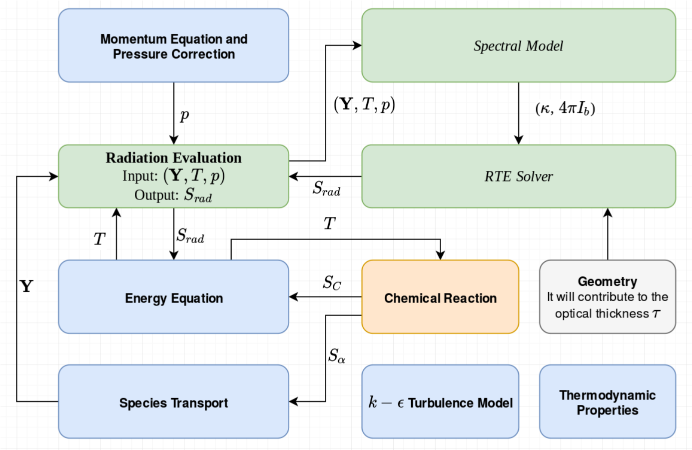

Figure : Schematic of the coupling between radiation and other sub-models

Example: Sandia Flame D×4 - RANS Simulation

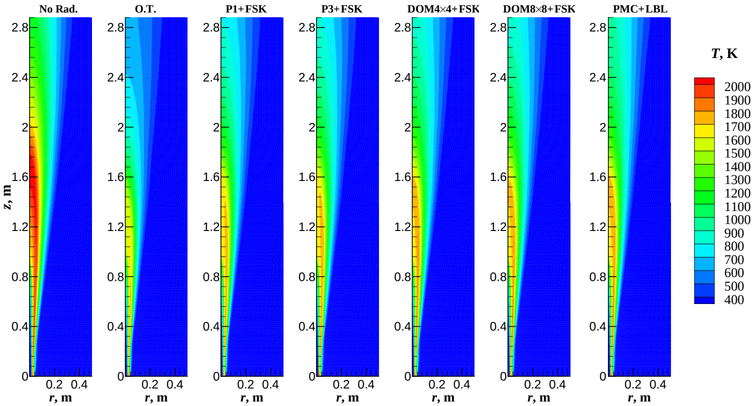

Figure : RANS Simulations of Sandia Flame D×4

- Not considering radiation will overpredict the peak temperature by up to 300 K
- Optically-thin model will underpredict the temperature about 200 K

Example: Aircraft Engine - LES Simulation

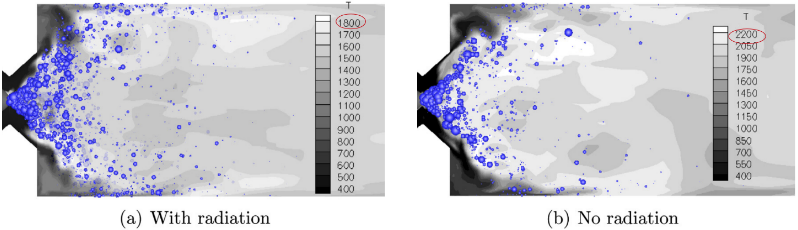

Figure : Droplet dist. sized by droplet mass and temp. dist. Source: CTR Standford and NASA, 2014

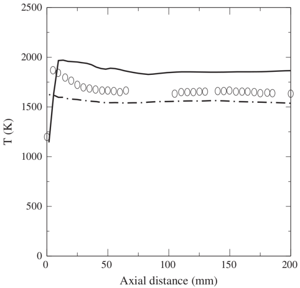

- No Rad. v.s. O.T. (gas phase)
- T_{peak} from O.T. is 400 K lower
- lower evaporation rates from O.T

Nongray radiation module

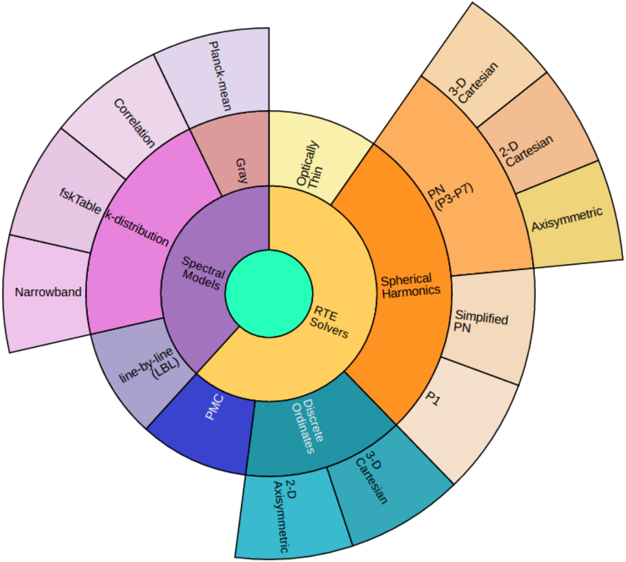

Outline

Summary of spectral models

- Gray model (Planck-mean)
  - Weighted average over the entire spectrum
  - Cheap, but inaccurate; Underpredict the absorption
  - In practice: most popular
- Band models
  - Constant properties over narrow or wide bands
  - Case dependent accuracy
  - In practice: popular, becoming less popular
- Full-spectrum k-distribution (FSK) or similar models (WSGG)
  - Reordering reoccuring spectral absorption coefficients
  - Very accurate; implementation dependent
  - In practice: less popular, becoming more popular
- Line-by-line (LBL) Calculations
  - The most accurate
  - Only practical for stochastic solution methods (PMC)
  - In practice: becoming more popular with Monte Carlo solution method

Gray model: constant absorption coefficient

Weighting the spectral absorption coefficient κ_η with the Planck function $I_{b\eta}$:

Planck-mean absorption coefficient:

$$\kappa_P = \frac{\int_0^\infty \kappa_\eta I_{b\eta} \mathrm{d}\eta}{\int_0^\infty I_{b\eta} \mathrm{d}\eta} = \frac{\int_0^\infty \kappa_\eta I_{b\eta} \mathrm{d}\eta}{\sigma_{SB} T^4}$$

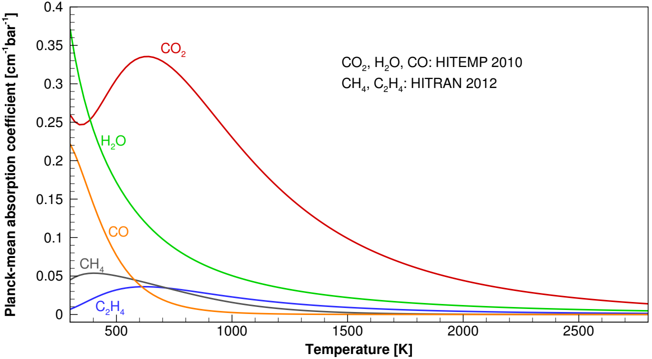

Figure : Planck-mean absorption coefficients of CO_2, H_2O, CO, CH_4 and C_2H_4

Full-spectrum k-distribution (FSK) model: reordering reoccuring κ_η

- Reduce the number of evaluations of the RTE required from 1 million to 8∼16.

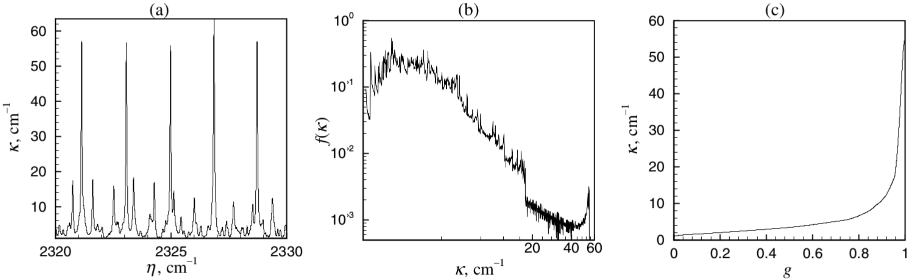

Figure : (a) Spectral absorption coefficient (b) PDF and (c) k-distribution for 4.5 μm CO_2 band at T=1000 K and p=1 bar.

1. $\eta - \kappa_\eta$
2. $k - f(k), f(k)$ is a weighted sum of the number of points where $\kappa_\eta = k$
3. $g - k, g$ is the cumulative distribution function of $f(k)$

Comparison of different FSK implementations

- generate k-distributions for individual species
  - Narrowband database - very accurate, less memory, more runtime computing
  - Correlations - less accurate, less memory, less runtime computing
- generate k-distributions for the mixture
  - Look-up table - very accurate, more memory, less computing

Table : CPU time comparisons of generating 10,000 arbitrary k-distributions of mixtures.

Database	Mixing model	CPU Time (s)
Narrowband	Multiplication	1389.65
	MRmixing	5904.59
Correlations	Multiplication	0.41
	MRmixing	8.97
Look-up table	-	0.26

FSK Table for nonhomogeneous mixtures

Table : Precalculated thermodynamic states of the FSK look-up table.

Parameters	Range	Values	Number of points
Species	CO_2, H_2O and CO		3
Pressure (total)	0.1 ~ 0.5 bar 0.7 bar 1.0 ~ 14.0 bar 15.0 ~ 80.0 bar	Every 0.1 bar 0.7 bar Every 1.0 bar Every 5.0 bar	34
Gas temperature	300~ 3000 K	Every 100 K	28
Reference temperature	300~ 3000 K	Every 100 K	28
Mole fraction of CO_2	0.0 ~ 0.05 0.25 ~ 1.0	Every 0.01 Every 0.25	10
Mole fraction of H_2O	0.0 ~ 0.05 0.1 ~ 0.2 0.25 ~ 1.0	Every 0.01 Every 0.05 Evert 0.25	13
Mole fraction of CO	0.0 ~ 0.5	{0.0, 0.01, 0.05, 0.1, 0.25, 0.5 }	6

- The size of the table is about 5 GB.
- Apply dynamic loading to reduce memory demand.
- The look-up table can be customized for specific needs.

Summary of RTE solvers

- Optically Thin (O.T.)
  - No absorption, only consider emission
  - Cheap, only useful for optically thin media
  - In practice: currently most popular
- Discrete Ordinates Method (DOM) or similar concepts
  - Discretize the angular profile of intensity by several finite directions
  - Cheap and accurate for non-scattering media, suffers from ray effects and false scattering for scattering media or reflecting surfaces
  - In practice: very popular, available in most comercial CFD softwares, $\mathrm{DOM}_{8\times 8}$ is usually good enough
- Spherical Harmonics (P_N) Method
  - Approximate the angular profile of intensity by a truncated series of spherical harmonics (a spectral method)
  - Very accurate for optically thick media; not accurate when intensity is directionally anisotropic
  - In practice: P_1 is very popular, high-order P_N needs more research
- Photon Monte Carlo (PMC)
  - The most accurate and robust
  - Used to be considered impractical
  - In practice: becoming more and more popular

Truncated series of spherical harmonics of order N:

$$I(\boldsymbol{\tau}, \hat{\mathbf{s}}) = \sum_{n=0}^{N} \sum_{m=-n}^{n} I_n^m(\boldsymbol{\tau}) Y_n^m(\hat{\mathbf{s}}), \qquad Y_n^m(\psi, \theta) = \begin{cases} \cos(m\psi) P_n^m(\cos\theta) & \text{for} \quad m \geq 0 \\ \sin(|m|\psi) P_n^m(\cos\theta) & \text{for} \quad m < 0 \end{cases}$$

- Use spherical harmonics as bases for the angular profile of intensity
- Transform the RTE into equations of the intensity coefficients I_n^m

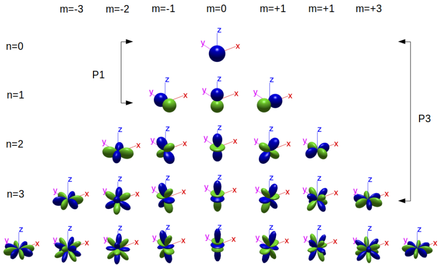

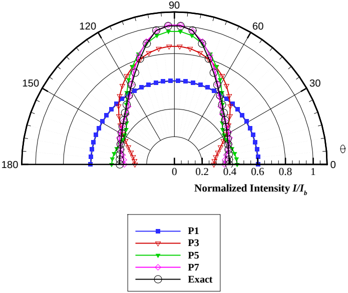

Governing equations

- Substitute the spherical harmonics series into the RTE;
- Multiply the resulting equation by Y_n^m and integrate the whole equation over a solid angle of 4π; One obtains $(N+1)^2$ first-order PDEs;
- The second-order elliptic formulation is obtained by eliminating the odd order intensity coefficients (I_n^m with odd n) by their relation to the gradients of I_{n+1}^m and I_{n-1}^m; This will reduce the number of governing equations to $N(N+1)/2$.

Table : Intensity coefficients employed for 3-D Cartesian formulation

n	Intensity Coefficients												
0							I_0^0						
2					I_2^{-2}	I_2^{-1}	I_2^0	I_2^1	I_2^2				
4			I_4^{-4}	I_4^{-3}	I_4^{-2}	I_4^{-1}	I_4^0	I_4^1	I_4^2	I_4^3	I_4^4		
6	I_6^{-6}	I_6^{-5}	I_6^{-4}	I_6^{-3}	I_6^{-2}	I_6^{-1}	I_6^0	I_6^1	I_6^2	I_6^3	I_6^4	I_6^5	I_6^6
n	I_n^{-n}	$\cdots$	$\cdots$	I_n^{-3}	I_n^{-2}	I_n^{-1}	I_n^0	I_n^1	I_n^2	I_n^3	$\cdots$	$\cdots$	I_n^n

For each $Y_n^m : n = 0, 2, \ldots, N-1,\ 0 \le m \le n$:

$$\sum_{k=1}^{3} \Bigg\{ (\mathcal{L}_{xx} - \mathcal{L}_{yy}) \left[(1+\delta_{m2}) a_k^{nm} I_{n+4-2k}^{m-2} + \frac{\delta_{m1}}{2} c_k^{nm} I_{n+4-2k}^{m} + e_k^{nm} I_{n+4-2k}^{m+2} \right]$$
$$+ (\mathcal{L}_{xz} + \mathcal{L}_{zx}) \left[(1+\delta_{m1}) b_k^{nm} I_{n+4-2k}^{m-1} + d_k^{nm} I_{n+4-2k}^{m+1} \right]$$
$$+ (\mathcal{L}_{xy} + \mathcal{L}_{yx}) \left[-(1-\delta_{m2}) a_k^{nm} I_{n+4-2k}^{-(m-2)} + \frac{\delta_{m1}}{2} c_k^{nm} I_{n+4-2k}^{-m} + e_k^{nm} I_{n+4-2k}^{-(m+2)} \right]$$
$$+ (\mathcal{L}_{yz} + \mathcal{L}_{zy}) \left[-(1-\delta_{m1}) b_k^{nm} I_{n+4-2k}^{-(m-1)} + d_k^{nm} I_{n+4-2k}^{-(m+1)} \right]$$
$$+ (\mathcal{L}_{xx} + \mathcal{L}_{yy} - 2\mathcal{L}_{zz}) c_k^{nm} I_{n+4-2k}^{m} \Bigg\}$$
$$+ \left[\mathcal{L}_{zz} - (1 - \omega\delta_{0n}) \right] I_n^m = -(1-\omega) I_b \delta_{0n}$$

where the operators: $\mathcal{L}_{xy} = \dfrac{1}{\beta}\dfrac{\partial}{\partial x}\left(\dfrac{1}{\beta}\dfrac{\partial}{\partial y}\right)$

Each governing equation is characterized by the spherical harmonics Y_n^m.

Marshak's boundary conditions

For each $\overline{Y}_{2i-1}^{\pm m}$, $i = 1, 2, \cdots, (N+1)/2$:

$$
\begin{aligned}
0 = &\sum_{l=0}^{\frac{N-1}{2}} \sum_{m'=-2l}^{2l} p_{2l,2i-1}^{m} \overline{\Delta}_{\pm m,m'}^{2l} I_{2l}^{m'} \\
&- \frac{\partial}{\partial \tau_{\overline{x}}} \sum_{l=l_1}^{\frac{N-1}{2}} \sum_{m'=-2l}^{2l} \left[(1 \pm \delta_{m,1}) u_{l,i}^{m} \overline{\Delta}_{\pm(m-1),m'}^{2l} - v_{l,i}^{m} \overline{\Delta}_{\pm(m+1),m'}^{2l} \right] I_{2l}^{m'} \\
&\pm \frac{\partial}{\partial \tau_{\overline{y}}} \sum_{l=l_2}^{\frac{N-1}{2}} \sum_{m'=-2l}^{2l} \left[(1 \mp \delta_{m,1}) u_{l,i}^{m} \overline{\Delta}_{\mp(m-1),m'}^{2l} + v_{l,i}^{m} \overline{\Delta}_{\mp(m+1),m'}^{2l} \right] I_{2l}^{m'} \\
&- \frac{\partial}{\partial \tau_{\overline{z}}} \sum_{l=0}^{\frac{N-1}{2}} \sum_{m'=-2l}^{2l} w_{l,i}^{m} \overline{\Delta}_{\pm m,m'}^{2l} I_{2l}^{m'}
\end{aligned}
$$

Each boundary condition is characterized by the local spherical harmonics $\bar{Y}_{2i-1}^{m}$.

I varies with r and axially with z, but not azimuthally with ϕ

$$I\,(r,\phi,z;\theta,\psi+\phi) = I\,(r,0,z;\theta,\psi)$$

$$I_n^m(r,\phi,z) = I_n^m(r,0,z)\cos m\phi = \hat{I}_n^m \cos m\phi$$

$$I_n^{-m}(r,\phi,z) = I_n^m(r,0,z)\sin m\phi = \hat{I}_n^m \sin m\phi$$

Employing the above relations to the general 3-D formulation, the number of governing equations is reduced to $(N+1)^2/4$ for axisymmetric geometry.

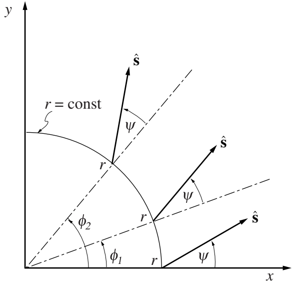

Table : Intensity coefficients employed for 2-D axisymmetric formulation

n	Intensity Coefficients						
0	$\hat{I}_0^0$						
2	$\hat{I}_2^0$	$\hat{I}_2^1$	$\hat{I}_2^2$				
4	$\hat{I}_4^0$	$\hat{I}_4^1$	$\hat{I}_4^2$	$\hat{I}_4^3$	$\hat{I}_4^4$		
6	$\hat{I}_6^0$	$\hat{I}_6^1$	$\hat{I}_6^2$	$\hat{I}_6^3$	$\hat{I}_6^4$	$\hat{I}_6^5$	$\hat{I}_6^6$
n	$\hat{I}_n^0$	$\hat{I}_n^1$	$\hat{I}_n^2$	$\hat{I}_n^3$	$\cdots$	$\cdots$	$\hat{I}_n^n$

- Specified radiative flux at the wall;
- Symmetry/specular reflection boundaries;
- Mixed diffuse-specular reflection surfaces;
- Cyclic boundaries.

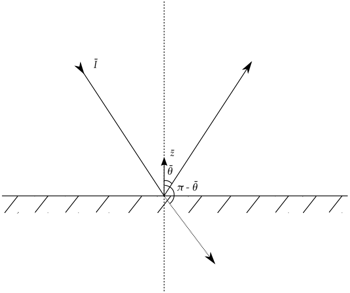

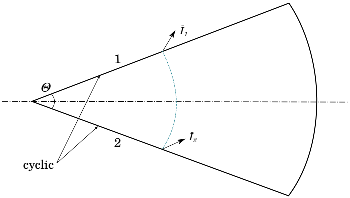

- Implementation platform → `OpenFOAM`® 2.2.x
- The spatial discretization → standard second-order finite volume method
- Solution method → segregated iterative method
- Solution of each governing equation (inner iterations) → the incomplete Cholesky preconditioned conjugated gradient method (PCG)
- Resolving the coupling between governing equations and Robin-type BCs (outer iterations) → Gauss Seidel method

Outline

Problem 1: 1-D slab with homogeneous radiative properties

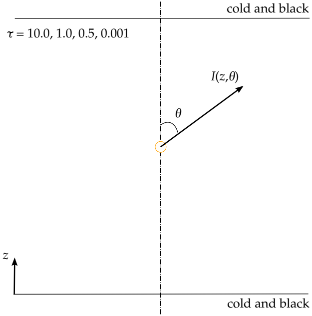

- 1-D Cartesian examples represent the radiative transfer between two infinitely long parallel plates;
- Geometry: 1-D Slab (1×1×101);
- All properties are normalized so that the only difference is the optical thickness;
- $-\nabla \cdot \mathbf{q}$ and G from P_1 to P_7 are compared to exact solution;
- Intensity I is reconstructed at the center ($z/L = 0.5$) and is also compared with the exact intensity.

τ=10 (Optically thick):

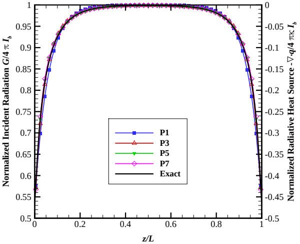

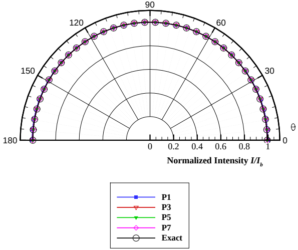

τ=1: (Optically intermediate):

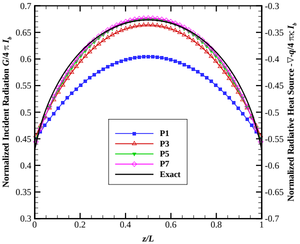

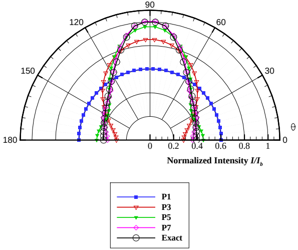

τ=0.5 (Optically intermediate):

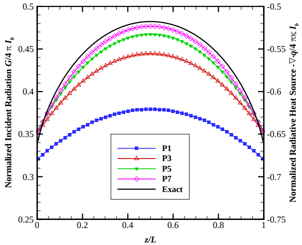

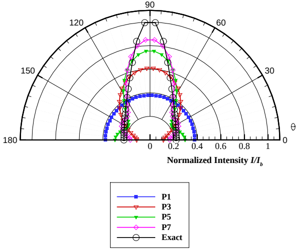

τ=0.001 (Optically thin):

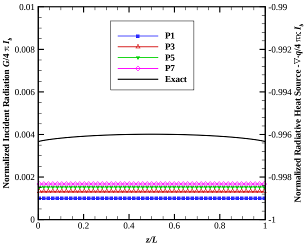

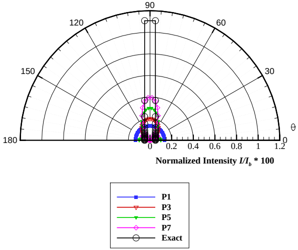

Problem 2: 1-D slab with flame-like variable radiative properties

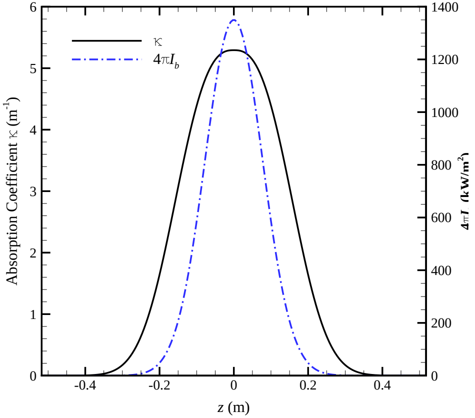

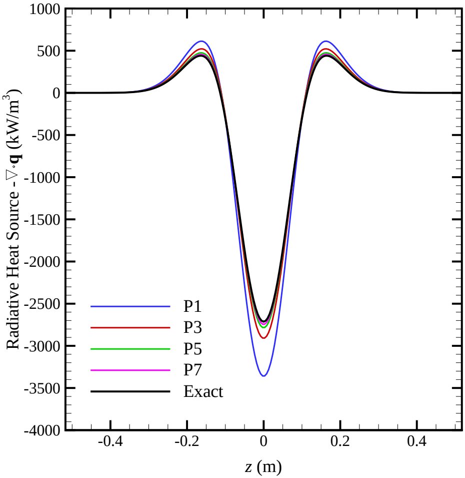

Geometry: 1-D Slab (200 cells), L=0.52×2 m;

Rotational invariance and comparison with PMC

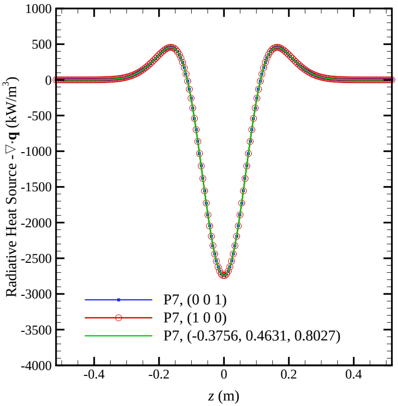

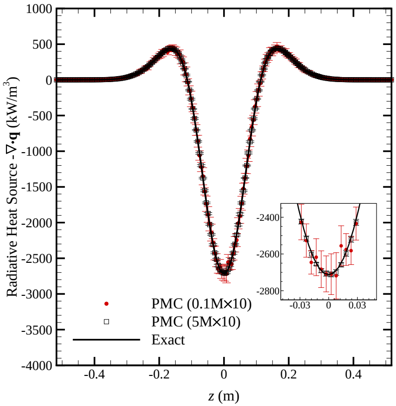

Table : Comparison of CPU time (s)

Num. of cells	τ_L	P_1	P_3	P_5	P_7	PMC (0.1M×10)	PMC (5M×10)
200	0.886	0.01	0.10	0.52	1.34	45.7	2532.1

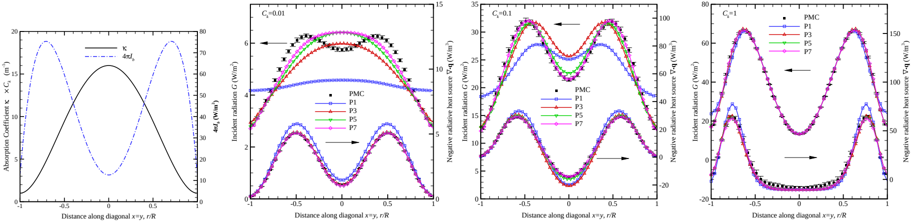

Table : Comparison of CPU time (s)

No. of cells	C_k	τ_R	P_1	P_3	P_5	P_7	PMC
2,601 (51×51)	C_k=1	12.7	0.02	0.75	4.71	7.0	459 (5M×10)
	C_k=0.1	1.27	0.02	0.87	5.05	9.33	125.5 (0.5M×10)
	C_k=0.01	0.127	0.02	1.78	7.09	19.2	21.2 (0.05M×10)

Problem 4: A 45-degree wedge and a full cylinder

$$I_b = 1 + \frac{20}{R^4} r^2 (R^2 - r^2) \quad \mathrm{W \cdot m^{-3}}$$

$$\kappa = \left[1 + \frac{15}{R^4}(R^2 - r^2)^2\right]\left(1 + 0.5\frac{r}{R}\cos 8\theta\right), \quad \mathrm{m^{-1}}$$

$$0 \le r \le R = 0.5, \quad \mathrm{m}$$

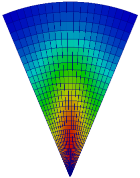

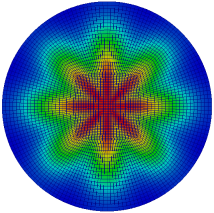

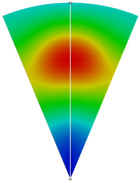

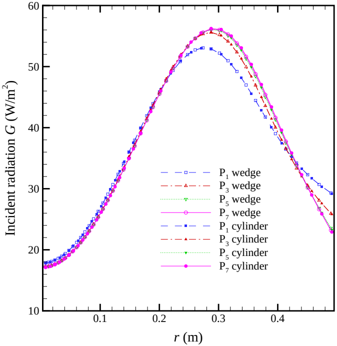

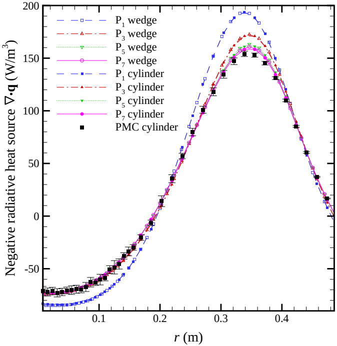

Coupled RANS Simulation - Sandia Flame D×4

- Sandia Flame D is a turbulent piloted jet flame with a Reynolds number of Re_D=22,400
- Fuel: Methane
- Diameter of main jet: d_j=7.2 mm
- The flame is scaled up to show radiation effects.

	Sandia Flame D		Sandia Flame D×4	
	d (mm)	u (m/s)	d (mm)	u (m/s)
main jet	7.2	49.89	28.8	12.4725
pilot	18.864	10.57	75.456	2.6425
co-flow	258.2	0.90	1032.8	0.2250

- Chemistry model: GRI-Mech 2.11 (49 species and 277 reactions), PaSR (partially-stired reactor)
- Turbulence model: Standard two-equation k–ϵ model
- Radiation models: O.T., PN+FSK, DOM+FSK, PMC+LBL

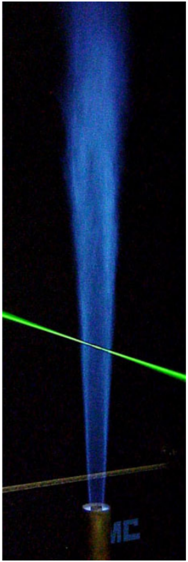

Source: Sandia NL

Temperature profiles along the axis - Sandia Flame D×4

Temperature profiles along the axis after the flame reaches steady state:

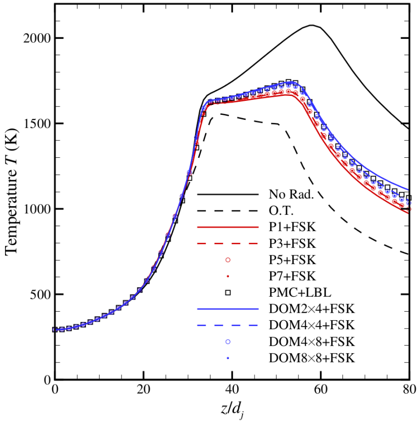

Radiation Solvers	$T_{p,c}$ (K)	$\Delta T_{p,c}$ (K)
No Rad.	2074	/
O.T.	1554	-520
P1+FSK	1666	-408
P3+FSK	1683	-391
P5+FSK	1688	-386
P7+FSK	1689	-385
DOM 2×4	1744	-330
DOM 4×4	1736	-338
DOM 4×8	1724	-350
DOM 8×8	1721	-353
PMC+LBL	1745	-329

- Adding radiation models cools down the flame and results in around 3% less-complete combustion.
- Nearly 30% of the combustion heat release is transfered to the environment through radiation.

Computational cost

Table : Average CPU time per time step (radiation is evaluated once per 1/10/100/250 time steps for the PN/DOM+FSK solvers and the average $t_{RTE} + t_{overhead}$ and t_{FSK} are only shown for runs with radiation evaluated once per time step)

Radiation Solver	Average CPU Time (s)	t_{RTE}+$t_{overhead}$ (s)	t_{FSK} (s)	
No Rad	0.82	/	/	
P1+FSK	0.97/0.85/0.82/0.82	0.09	0.06	1 second-order PDE
P3+FSK	1.05/0.87/0.83/0.83	0.17		4 second-order PDE
P5+FSK	1.36/0.88/0.84/0.84	0.48		9 second-order PDE
P7+FSK	1.64/0.90/0.85/0.85	0.76		16 second-order PDE
DOM 2×4+FSK	1.11/0.86/0.85/0.84	0.23		8 first-order PDE
DOM 4×4+FSK	1.20/0.87/0.85/0.84	0.32		16 first-order PDE
DOM 4×8+FSK	1.42/0.91/0.86/0.86	0.54		32 first-order PDE
DOM 8×8+FSK	1.78/0.94/0.87/0.87	0.9		64 first-order PDE
PMC+LBL	0.87	0.05	/	5,000 with time-blending
PMC+LBL	0.92	0.10	/	10,000 with time-blending

All computations are performed on twelve 2.66 GHz Intel Xeon X7460 processors.

A mixture of hot CO_2, H_2O and CO:

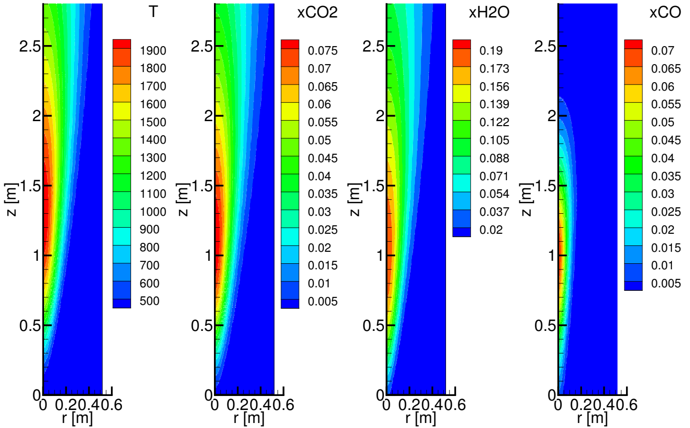

Spectral model for P_N and DOM: FSK-Table with eight quadrature points
Spectral model for for PMC: LBL

Grids

- Radiative calculations are conducted on a 2-D wedge, a 3-D cylinder and a 3-D cuboid
- The same axisymmetric distributions of temperature and mole fractions

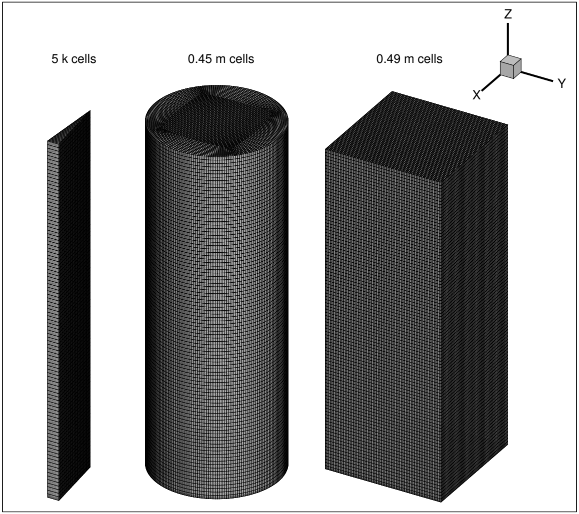

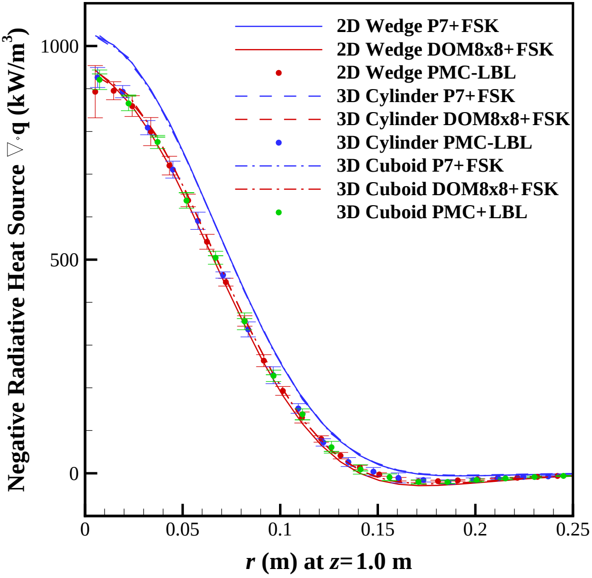

2D Wedge P7+FSK
2D Wedge DOM8x8+FSK
2D Wedge PMC-LBL
3D Cylinder P7+FSK
3D Cylinder DOM8x8+FSK
3D Cylinder PMC-LBL
3D Cuboid P7+FSK
3D Cuboid DOM8x8+FSK
3D Cuboid PMC+LBL
Negative Radiative Heat Source ∇·q (kW/m³)
1000
500
0
0
0.05
0.1
0.15
0.2
0.25
r (m) at z=1.0 m

Negative radiative heat source $\nabla \cdot \mathbf{q}$ from different RTEs

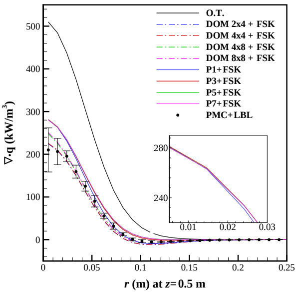

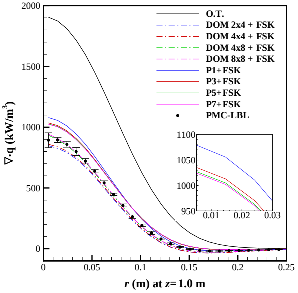

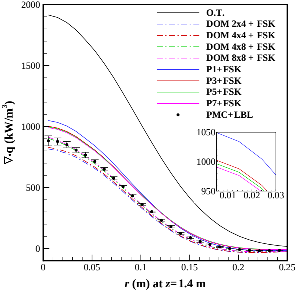

Table : Optical thickness $\tau_{R,g}$ along radius at $z = 1.0$ m for each quadrature point

Index	1	2	3	4	5	6	7	8
$\tau_{R,g}$	0.0006	0.0035	0.0120	0.03348	0.08081	0.2112	0.8327	3.5118

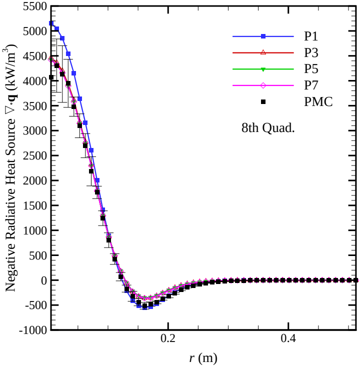

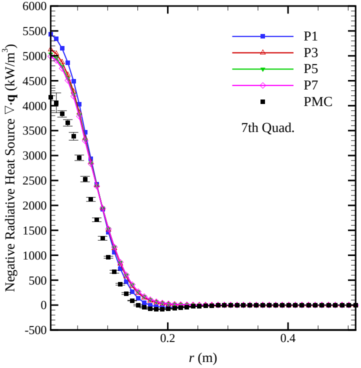

Oxy-fuel combustion is the process of burning a fuel using pure oxygen instead of air as the primary oxidant. A 0.8 MW oxy-natural gas burner (OXYFLAM-2A) from the OXYFLAME project:

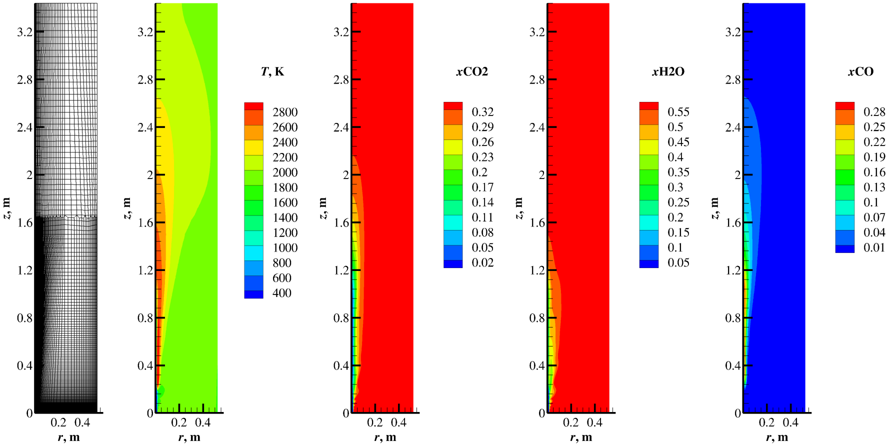

Gray Spectral Model, $z = 1.42$ m

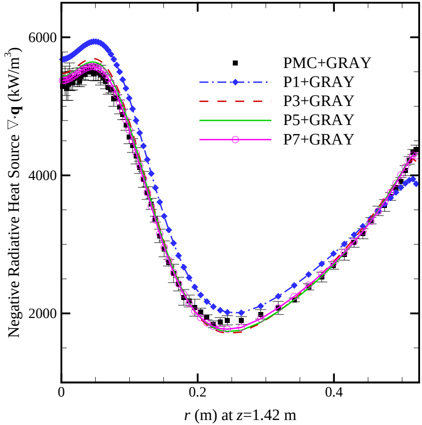

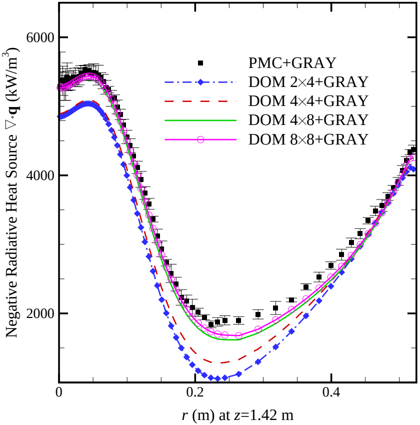

Table : Comparison of CPU time (s) of the RTE solvers for the gray case

	P_1	P_3	P_5	P_7	$DOM_{2\times4}$	$DOM_{4\times4}$	$DOM_{4\times8}$	$DOM_{8\times8}$	PMC
Gray	0.22	2.95	10.2	27.8	4.53	5.45	6.66	13.9	223 (1M×10)

FSK Spectral Model, $z = 1.42$ m

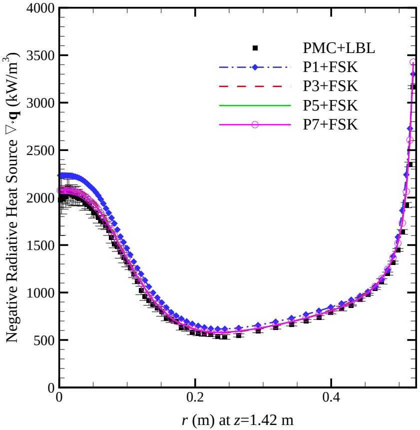

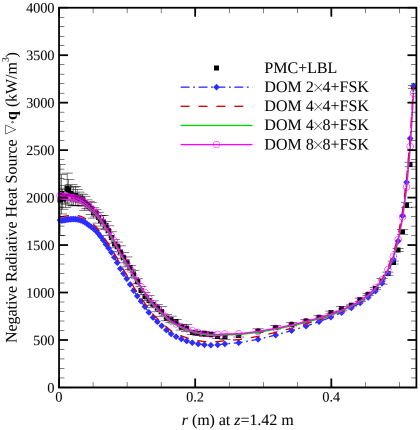

Table : Comparison of CPU time (s) of the RTE solvers for the nongray case

	P_1	P_3	P_5	P_7	$DOM_{2\times4}$	$DOM_{4\times4}$	$DOM_{4\times8}$	$DOM_{8\times8}$	PMC
Nongray	0.95	12.8	49.7	111	13.1	25.8	39.4	77.5	1672 (10M×10)

Acknowledgements:

Prof. Michael Modest, University of California, Merced
Prof. Daniel Haworth, Pennsylvania State University
Prof. Somesh Roy, Marquette University
Dr. Tao Ren, University of California, Merced
Prof. Xinyu Zhao, University of Connecticut

J. Quant. Spectrosc. Radiat. Transfer. Vol. 15, pp. 445–461. Pergamon Press 1975. Printed in Great Britain

RADIATIVE EQUILIBRIUM IN A RECTANGULAR ENCLOSURE BOUNDED BY GRAY WALLS

MICHAEL F. MODEST*

National Research Council, NASA-Lyndon B. Johnson Space Center, Houston, Texas 77058, U.S.A.

(*Received* 26 *April* 1974)